Intramolecular Electron Transfer and Conformational Changes in Cytochrome *c* Oxidase†

Ólöf Einarsdóttir,* Katy E. Georgiadis, and Artur Sucheta

Department of Chemistry, University of California, Santa Cruz, California 95064

Received August 22, 1994; Revised Manuscript Received November 1, 1994®

ABSTRACT: The photolysis intermediates of partially and fully reduced CO-bound cytochrome oxidase derivatives were investigated. A gated optical spectrometric multichannel analyzer was used to collect visible and near-infrared transient difference spectra on time scales from nanoseconds to milliseconds. The spectra were analyzed by a singular value decomposition method combined with a global exponential fitting procedure. Global analysis of the mixed-valence CO complex transient difference spectra shows that five intermediates are present with apparent lifetimes of 1.4 μs, 4.8 μs, 76.7 μs, 10.6 ms, and 21.6 ms. The data were fitted to a kinetic model involving a sequential pathway with accompanying equilibria. On the basis of this mechanism, the absorption spectra of the intermediates were determined. The first step, also present in the fully reduced enzyme, is attributed to a conformational change at cytochrome a_3. The spectral changes associated with the second step are similar to those expected for 1:1 electron transfer from cytochrome a_3 to cytochrome *a*, except for a higher absorbance between 480 and 550 nm. A comparison of the experimental spectral change associated with this step, (a^{2+} minus a^{3+}) minus (a_3^{2+} minus a_3^{3+}), and the calculated spectral change, (a^{2+} Cu_A^{+} minus a^{3+} Cu_A^{2+}) minus (a_3^{2+} Cu_B^{+} minus a_3^{3+} Cu_B^{2+}), allowed extraction of the absorbance spectrum of Cu_A^{2+} in the 480−550 nm region. The spectral change associated with the third step is consistent with the oxidation of cytochrome *a*. A decrease in the 830 nm band on the same time scale indicates that the electron acceptor is Cu_A. The data also suggest that the redox state of Cu_B significantly affects the absorption spectrum of oxidized cytochrome a_3 in the visible region. The two processes on a millisecond time scale are attributed to CO recombination and intramolecular electron transfer.

Intramolecular electron transfer in cytochrome oxidase can be investigated by photolyzing CO from the mixed-valence CO complex (cytochrome a_3^{2+}−CO Cu_B^{+} cytochrome a^{3+} Cu_A^{2+})[1] (Boelens & Wever, 1979; Boelens et al., 1982; Brzezinski & Malmström, 1987; Morgan et al., 1989; Oliveberg & Malmström, 1991; Einarsdóttir et al., 1992a; Verkhovsky et al., 1992; Georgiadis et al., 1994; Hallén et al., 1994) and the three-electron-reduced CO compound (Morgan et al., 1989; Oliveberg & Malmström, 1991). The apparent reduction potential of the binuclear site is lowered upon CO photolysis, leading to electron transfer from the binuclear site to the low potential redox centers, cytochrome *a* and Cu_A (Boelens & Wever, 1979; Boelens et al., 1982). Oliveberg and Malmström (1991) observed two processes at 445 and 605 nm, with apparent rates of 2×10^5 s^{-1} and 1.3×10^4 s^{-1}, following photolysis of the mixed-valence CO enzyme. The two processes were attributed to electron transfer between cytochrome a_3 and cytochrome *a* and between cytochrome *a* and Cu_A, respectively. By following electron transfer at individual wavelengths in the Soret region, Verkhovsky et al. (1992) reached similar conclusions. A slow phase (k_{app} ~500 s^{-1}) has also been reported by the Göteborg group (Brzezinski & Malmström, 1987; Oliveberg & Malmström, 1991; Hallén et al., 1994). This phase had been attributed to a structural change (Oliveberg & Malmström, 1991), but a more recent kinetic difference spectrum indicates that it is due to electron transfer from cytochrome a_3 to cytochrome *a* (Hallén et al., 1994). The phase was found to be sensitive to pH and D_2O, suggesting that it is coupled to proton transfer events.

In recent studies from our laboratory, intramolecular electron transfer in cytochrome oxidase was investigated in the Soret region following photolysis of the mixed-valence CO complex (Georgiadis et al., 1994). Time-resolved difference spectra were collected using a gated optical spectrometric multichannel analyzer (OSMA) system and analyzed by a global exponential fitting routine combined with a singular value decomposition method. Modeling of the data suggested that a conformational change at cytochrome a_3 preceded electron transfer from cytochrome a_3 to cytochrome *a* on an early microsecond time scale (Georgiadis et al., 1994). This was followed by electron transfer from cytochrome *a* to Cu_A in agreement with previous studies (Oliveberg & Malmström, 1991; Verkhovsky et al., 1992). The global analysis also indicated two millisecond processes.

A comparison of the experimental and predicted absorbance changes associated with the two electron transfer steps in the Soret region indicated some spectral interactions among the redox centers, but no major contribution due to the oxidized coppers was detected in this region (Georgiadis

† This work was supported by National Institutes of Health Grant GM45888.

* Author to whom correspondence should be addressed.

® Abstract published in *Advance ACS Abstracts,* December 15, 1994.

[1] Abbreviations: CcO, cytochrome *c* oxidase; SVD, singular value decomposition; b-spectrum, spectral changes associated with a particular first-order process; OSMA, optical spectrometric multichannel analyzer; k_{app}, apparent rate constant; τ, apparent lifetime; Cu_A, copper A; Cu_B, copper B; a^{2+}, reduced cytochrome *a*; a^{3+}, oxidized cytochrome *a*; a_3^{2+}; reduced cytochrome a_3; a_3^{3+}, oxidized cytochrome a_3.

0006-2960/95/0434-496$09.00/0

et al., 1994). Due to the intense $\pi \rightarrow \pi^*$ transitions of the hemes in the Soret and visible regions, extraction of the absorbance spectra of the oxidized coppers has been difficult. However, low-temperature magnetic circular dichroism measurements have shown a transition at ~520 nm which was attributed to Cu_A^{2+} (Greenwood et al., 1983, 1988; Thomson et al., 1986; Farrar et al., 1991). A visible spectrum with a maximum at ~530 nm has been reported for a Cu_A mutant of subunit II of cytochrome *bo* from *Escherichia Coli* (van der Oost et al., 1992; Kelly et al., 1993). Lappalainen et al. (1993) and von Wachenfeldt et al. (1994) recently obtained similar spectra for the Cu_A domains of cytochrome *c* oxidase from *Paracoccus denitrificans* and caa_3 oxidase from *Bacillus subtilis*, respectively. Therefore, several lines of evidence indicate that Cu_A^{2+} has an optical absorption in the visible region between 480 and 550 nm.

In this study, we probed transient absorbance changes in the visible and near-infrared regions following photolysis of CO bound to the mixed-valence, three-electron-reduced, and fully reduced complexes. The data are consistent with our previously reported mechanism involving a conformational change at cytochrome a_3, followed by electron transfer from cytochrome a_3 to cytochrome *a* with subsequent electron transfer to Cu_A (Georgiadis et al., 1994). Our data also provide evidence for an optical absorption due to Cu_A^{2+} in the 480−550 nm region and suggest that the redox state of Cu_B significantly affects the spectrum of oxidized cytochrome a_3.

MATERIALS AND METHODS

Cytochrome oxidase was isolated from fresh beef hearts according to the method of Yoshikawa et al. (1977) with a final dialysis against 0.1 M sodium phosphate buffer, pH 7.4. The mixed-valence CO complex was obtained by incubating a deoxygenated enzyme solution under CO for a few hours. The three-electron-reduced CO complex was made by a prolonged incubation (5−10 h) under CO. Enzyme concentration was determined spectrophotometrically using extinction coefficients of 8.5 mM^{-1} cm^{-1} at 598 nm for the oxidized enzyme or 19.9 mM^{-1} cm^{-1} at 604 nm for the reduced protein (Yoshikawa et al., 1977) and is expressed in terms of the concentration of cytochrome oxidase (i.e., 50% of the heme *a* concentration). The CO complexes were characterized by their visible spectra which were recorded before and after the photolysis measurements to ensure that the samples did not change during the measurements.

The CO complexes were photolyzed with a DCR-11 Nd:YAG laser (532 nm, 45 mJ/pulse). A 10 × 4 mm cuvette was used with the laser photolysis beam along the 4 mm path length and the probe beam along the 10 mm path length. The probe beam was a pulsed xenon flashlamp light source with time resolution of 4 μs (full width at half-maximum). The transient optical signals were detected by a gated optical spectrometric multichannel analyzer (OSMA) connected to the spectrograph's (Aries, FF250; 150 grooves/mm grating) output port. Further experimental details were provided in a previous paper (Georgiadis et al., 1994).

Global Data Analysis. The time-resolved data were analyzed at all wavelengths and times simultaneously as described previously (Georgiadis et al., 1994), combining exponential fitting and singular value decomposition (SVD) procedures (Hug et al., 1990; Thorgeirsson et al., 1991, 1992). The analysis consists of three steps carried out using Matlab software (Mathworks), the first of which is the SVD. The SVD procedure gives the minimum number of orthonormal basis spectra that are needed to represent the whole data set and thereby reduces the number of parameters required for the subsequent exponential fitting (Golub & Reinsch, 1970; Henry & Hofrichter, 1992). In the second stage of the analysis, the reduced data set is fitted to a sum of exponentials. The output of this process are the apparent (observed) rate constants, k_i, and the spectral changes associated with the apparent rates, or the b-spectra (Hug et al., 1990; Thorgeirsson et al., 1991, 1992). The number of exponentials constituting the fitted linear combination was increased until a random pattern was obtained in the plot of the residuals as a function of both wavelength and time. Further details of the data analysis have been reported previously (Hug et al., 1990; Thorgeirsson et al., 1991, 1992; Georgiadis et al., 1994).

The final step in the spectral analysis involves testing different mechanisms by extracting the spectra of the intermediates based on a set of microscopic rate constants (Georgiadis et al., 1994). Alternatively, b-spectra and apparent lifetimes can be calculated if the spectra of all the intermediates and the microscopic rate constants are known. A comparison of the experimental and calculated b-spectra and the corresponding apparent lifetimes then provides a criterion for the validity of a given kinetic model (Hug et al., 1990; Thorgeirsson et al., 1991, 1992; Georgiadis et al., 1994). In the present study, model spectra of the intermediates were appropriate linear combinations of the ground state spectra of the oxidized, fully reduced, mixed-valence CO and fully reduced CO enzyme complexes. Calculated b-spectra were obtained from the model spectra of the intermediates using optimized values of the microscopic rate constants. For each mechanism tested, the microscopic rate constants were varied iteratively by the simplex optimization algorithm. The search terminated when a set of microscopic rate constants gave a local minimum of the following weighted sum of relative deviations:

$$s = w_{\text{spec}} \sum_{i=1}^{k} \sum_{\lambda} \left(\frac{b(\lambda)_{\text{data},i} - b(\lambda)_{\text{calc},i}}{\sigma_{\text{spec}}} \right)^2 + w_{\text{time}} \sum_{i=1}^{k} \left(\frac{1}{\delta} \frac{\tau_{\text{data},i} - \tau_{\text{calc},i}}{\tau_{\text{data},i}} \right)^2 \quad (1)$$

where k is the number of apparent rates, $b(\lambda)_{\text{data}}$ and $b(\lambda)_{\text{calc}}$ are the experimental and calculated b-spectra, respectively, and τ_{data} and τ_{calc} are the experimental and calculated apparent lifetimes, respectively. The weighting factors, w_{spec} and w_{time}, serve to normalize the contributions to s from the residuals arising from the b-spectra and apparent lifetimes, respectively. The value of s is affected to a much greater extent by the discrepancy between the experimental and calculated b-spectra than by the corresponding difference in the lifetimes. This is due to the number of parameters involved in the b-spectra, $(k + 1) \times m$ (where m is the number of wavelengths monitored), compared to k parameters in case of the apparent lifetimes. The factor δ is an estimate of the average relative error in each τ. Its value was assumed to be identical to the tolerance used as the convergence criterion

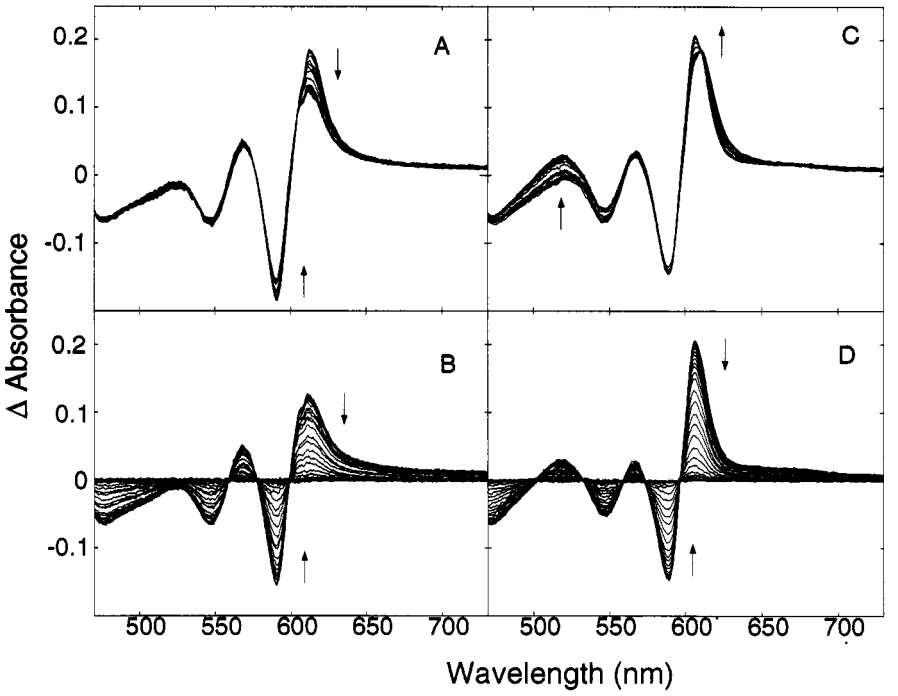

FIGURE 1: Transient absorption difference spectra of fully reduced CO−cytochrome *c* oxidase (A and B) and mixed-valence CO−cytochrome *c* oxidase (C and D) in the visible region. The spectra were obtained at 55 delay times between 40 ns and 300 ms after CO photolysis. The number of delay times in each time decade were as follows: 10 between 40 ns and 1 μs, 6 between 1 and 10 μs, 9 between 10 and 100 μs, 9 between 100 μs and 1 ms, 8 between 1 ms and 10 ms, and 13 between 10 and 300 ms. Each spectrum represents 128 accumulated averages. The cytochrome oxidase concentration was 43 μM in 0.1 M sodium phosphate buffer (pH 7.4) at 24 °C. The CO concentration was 1 atm.

in the previous multiexponential fitting step. In the process of evaluating various mechanisms, several starting sets of the microscopic rate constants were tested in order to assure that the local minimum was the "best" minimum attainable. If multiple minima were detected, a direct comparison of the resultant *s* values was used to determine the most appropriate values for the microscopic rate constants.

RESULTS

Visible Region: (A) Fully Reduced CO−Cytochrome c Oxidase. The transient absorption difference spectra following photolysis of the fully reduced CO complex are shown in Figure 1 (panels A and B). The spectra, which represent the absorbance of the photoproducts minus that of the unphotolyzed fully reduced CO complex, were collected at 55 time delays between 40 ns and 300 ms after CO photolysis. The peak in the 40 ns difference spectrum is at ~614 nm and the trough at ~592 nm. The peak has a significantly higher intensity than the corresponding peak in the difference spectrum of the fully reduced unliganded enzyme and the fully reduced CO complex. The transient difference spectra show a substantial decrease and a small blue shift (~1−2 nm) in the α band between 40 ns and 25 μs following CO photolysis (Figure 1A). The microsecond changes are followed by the CO recombination on a millisecond time scale (Figure 1B).

Global exponential fitting analysis of the transient difference spectra supports the presence of two processes with apparent lifetimes of 1.5 μs and 11 ms. Figure 2A shows the spectral changes (b-spectra) associated with the two processes. The residual spectra from the two-exponential fit (the difference between the transient data and the fit) are shown in Figure 2B. The residuals show primarily random

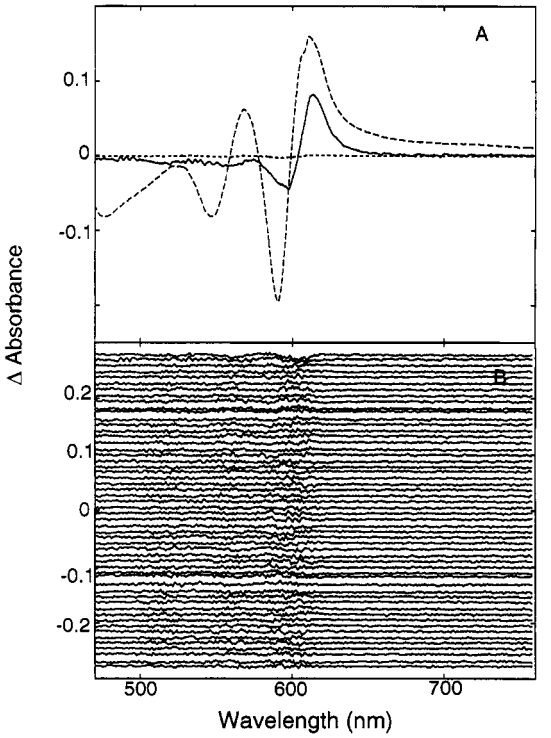

FIGURE 2: (A) Spectral changes (b-spectra) associated with the two lifetimes, 1.5 μs (solid) and 11.0 ms (dashed), from a two-exponential fit of the time-resolved data of the fully reduced CO complex (Figure 1A,B). (B) Residuals (data minus fit) from a two-exponential fit of the time-resolved data of the fully reduced CO complex. The residuals are separated by a constant factor and are plotted on the indicated absorbance scale.

structure; however, it was found that, upon addition of one more lifetime, τ ~200 μs, the total residual was decreased further. The amplitude of the corresponding b-spectrum was

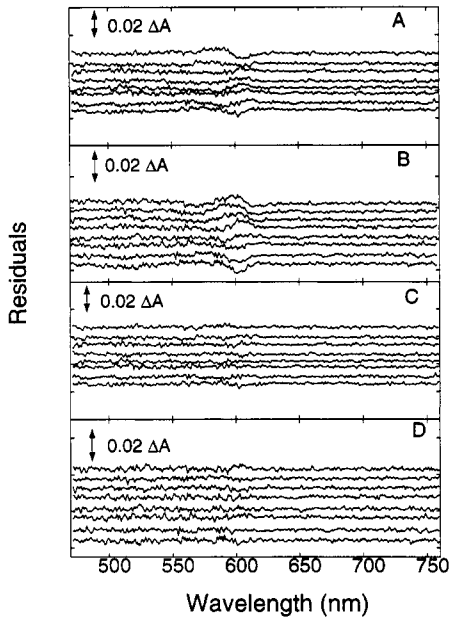

FIGURE 3: Subset of residuals (data minus fit) on microsecond and millisecond time scales from (A and B) a three-exponential fit (τ_{app} = 1.8 μs, 50.8 μs, and 15.4 ms) and (C and D) a five-exponential fit (τ_{app} = 1.4 μs, 4.8 μs, 76.7 μs, 10.6 ms, and 21.6 ms) of the mixed-valence CO complex transient data in Figure 1, panels C and D. The residuals are separated by a constant factor. Each line (from top to bottom) represents the absorbance difference of the data and the least-squares fit at the following time points after photodissociation of CO from cytochrome a_3: (A and C) 3, 5, 10, 16, 28, 47, 80, and 130 μs and (B and D) 9, 15, 25, 43, 72, 130, 240, and 300 ms.

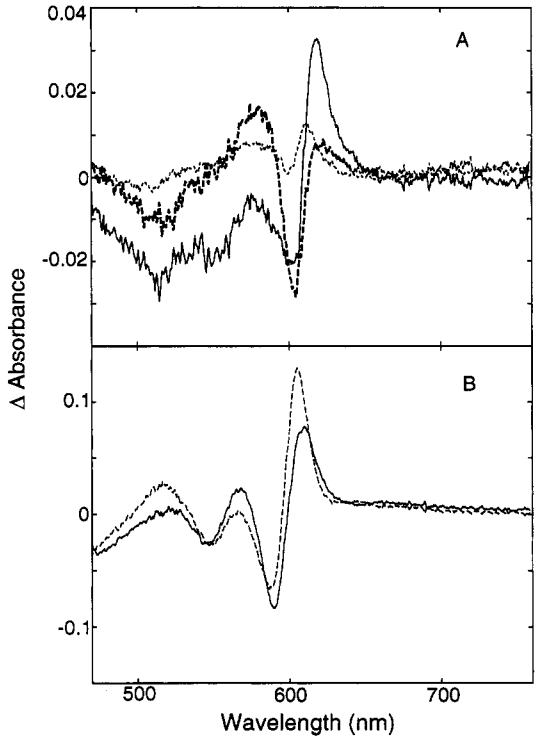

FIGURE 4: Spectral changes (b-spectra) from the five-exponential fit of the mixed-valence CO complex transient data (Figure 1C,D). (A) The b-spectra associated with the first three lifetimes, 1.4 μs (solid line), 4.8 μs (bold dotted line), and 77 μs (unbold dotted line). (B) The b-spectra associated with the two millisecond processes, 10.6 ms (solid line) and 21.6 ms (dashed line).

very small, and therefore this process was omitted in further analysis.

Visible Region: (B) Mixed-Valence CO−Cytochrome Oxidase. Figure 1 (panels C and D) shows the transient difference spectra in the visible region following photolysis of CO from the mixed-valence CO complex. The peak in the 40 ns transient difference spectrum of the mixed-valence CO compound is at ~611 nm and the trough at ~591 nm. It is clear that the spectral changes on an early time scale (40 ns−25 μs) are not the same for the fully reduced CO complex (Figure 1A) and the mixed-valence CO derivative (Figure 1C). The transient difference spectra of the mixed-valence CO complex show a blue shift and a slight increase in the intensity of the α band on an early microsecond time scale. This is accompanied by a substantial increase at ~520 nm (Figure 1C), indicative of the reduction of cytochrome *a*. The transient difference spectra also show a small increase at 675 nm on a microsecond time scale (τ ~1−5 μs). Figure 1D shows the transient absorbance changes between 25 μs and 300 ms following photolysis of the mixed-valence CO enzyme.

The transient difference spectra of the mixed-valence CO complex (Figure 1C,D) were analyzed using a combination of global exponential fitting and SVD. Based on the relative magnitude of the first few singular values [9.6, 1.2, 0.275, 0.108, 0.095, 0.0479, 0.0355, 0.0329, ... (55 singular values total)], which provide an estimate of the number of intermediates present, global fits assuming three, four, and five intermediates (not counting the final product, the mixed-valence CO complex) were compared. The residuals from a three-exponential fit of the data in Figure 1, panels C and D, are shown in Figure 3, panels A and B, for selected time points in the microsecond and millisecond time regimes, respectively. The corresponding apparent lifetimes were 1.8 μs, 50.8 μs, and 15.4 ms. The residuals on both microsecond and millisecond time scales display a nonrandom pattern implying that additional processes occur on these time scales (Figure 3A,B). The residuals from a five-exponential fit of the mixed-valence CO complex transient difference spectra are shown in Figure 3, panels C and D, for the microsecond and millisecond time scales, respectively. It is clear that the nonrandom pattern present in the residuals resulting from a three-exponential fit (Figure 3A,B) has disappeared. The apparent lifetimes from the five-exponential fit were 1.4 μs, 4.8 μs, 76.7 μs, 10.6 ms, and 21.6 ms. These lifetimes are almost identical within experimental error to those obtained using a five-exponential fit on the transient difference spectra of the mixed-valence CO complex in the Soret region (Georgiadis et al., 1994). The b-spectra associated with the three microsecond and two millisecond processes are shown in Figure 4, panels A and B, respectively.

Visible Region: (C) Three-Electron-Reduced CO−Cytochrome Oxidase. Figure 5 (panels A and B) shows absorbance changes following photolysis of the three-electron-reduced CO complex. The transient difference spectra are similar, but not identical, to those of the mixed-valence CO complex. This is reflected in the b-spectra (Figure 5C,D) resulting from a five-exponential fit of the transient data, which show different relative intensities compared to those of the mixed-valence CO compound (Figure 4A,B). The apparent lifetimes of the five processes in the three-electron-reduced CO complex were 1.2 μs, 5.2 μs, 77.6 μs, 8.7 ms, and 18.3 ms.

Near-Infrared Region. Figure 6 shows transient absorbance changes in the near-infrared region following pho-

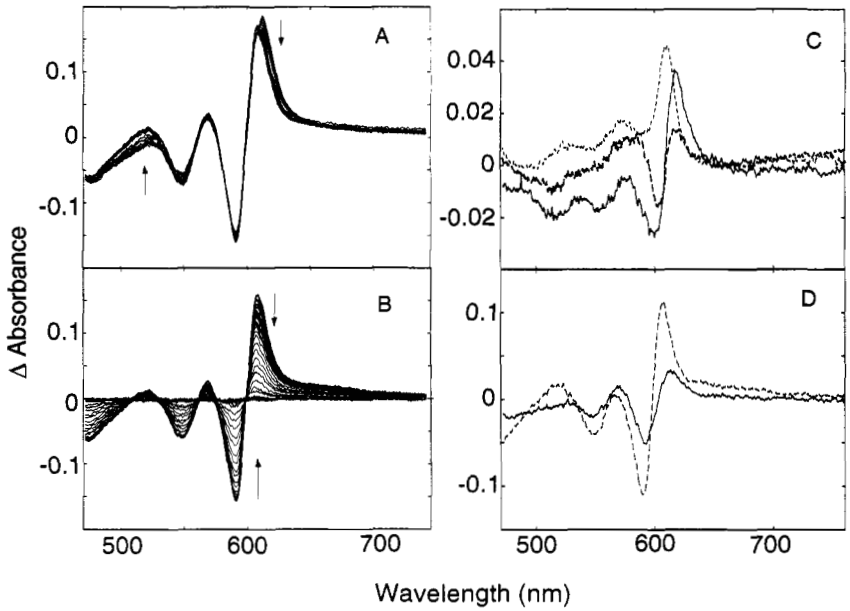

FIGURE 5: (A and B) Transient absorption difference spectra of three-electron-reduced CO−cytochrome *c* oxidase between 30 ns and 20 μs (A) and 25 μs and 300 ms (B) after photolysis of CO from cytochrome a_3. The spectra were collected at 54 delay times after the laser pulse with the number of time points in each decade similar to that described in Figure 1. (C and D) Spectral changes (b-spectra) from a five-exponential fit of the three-electron-reduced CO complex transient data. (C) The b-spectra associated with the first three lifetimes, 1.2 μs (solid line), 5.2 μs (bold dotted line), and 77.6 μs (unbold dotted line). (D) The b-spectra associated with the two millisecond processes, 8.7 ms (solid line) and 18.3 ms (dashed line). The concentration of oxidase and conditions were the same as those listed in Figure 1.

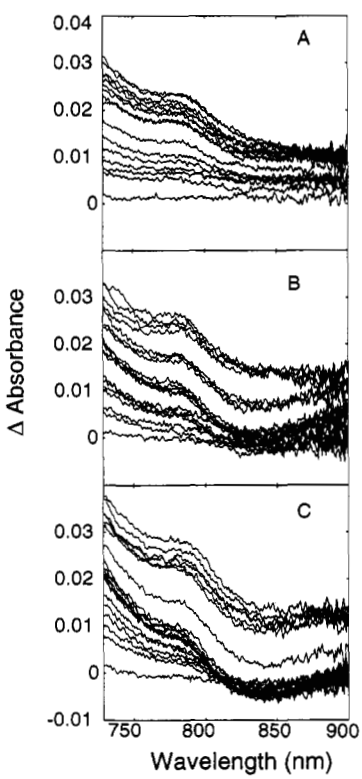

FIGURE 6: Transient absorption difference spectra in the near-infrared region following photolysis of CO from (A) the fully reduced CO, (B) the mixed-valence CO, and (C) the three-electron-reduced CO enzyme derivatives. Cytochrome oxidase concentration was 160 μM in 0.1 M sodium phosphate buffer (pH 7.4) at 24 °C. The CO concentration was 1 atm.

tolysis of (A) the fully reduced CO, (B) the mixed-valence CO, and (C) the three-electron-reduced CO derivatives (C). There is a decrease at ~830−840 nm on a microsecond time scale (τ ~50−100 μs) in the transient difference spectra of the mixed-valence and three-electron-reduced enzyme CO derivatives (Figure 6B,C), reflective of the reduction of Cu_A (Wharton & Tzagoloff, 1964; Beinert et al., 1980). The apparent lifetime of this process (τ ~50−100 μs) is similar to the 77 μs apparent lifetime observed in the visible region, indicating that both phases represent the same electron transfer process. The three-electron-reduced CO compound shows a significantly larger absorbance decrease at 830 nm (Figure 6C) than the mixed-valence CO complex (Figure 6B) in agreement with previous studies by Oliveberg and Malmström (1991). As expected, no absorbance decrease is observed at 830 nm on a microsecond time scale following photolysis of the fully reduced CO complex (Figure 6A).

A band at 785 nm is observed in the transient difference spectra of all three complexes (Figure 6). We previously attributed this band, which disappears on the time scale of the CO recombination, to the unliganded five-coordinate high-spin cytochrome a_3^{2+} (Einarsdóttir et al., 1992b). This conclusion is consistent with a previous magnetic circular dichroism assignment of this band (Eglinton et al., 1980) and recent studies by Rich and co-workers on cytochrome aa_3 (Rich et al., 1992) and cytochrome *bo* from *E. coli* (Ingledew et al., 1992).

DISCUSSION

Photolysis of the Fully Reduced CO Complex. The microsecond and millisecond processes observed in the CO photodissociation dynamics of the fully reduced CO enzyme can be represented by Scheme 1 (Woodruff et al., 1991; Einarsdóttir et al., 1993; Georgiadis et al., 1994). On the basis of this mechanism, the microscopic rate constants in Table 1, and the b-spectra, the difference spectra of the intermediates, i.e., the spectra of the intermediates minus the spectrum of the unphotolyzed fully reduced CO complex, were determined. These are shown in Figure 7A. As noted above, the difference spectrum of intermediate **I** (Figure 7A,

Table 1

	rate constants		equilibrium constants
	Scheme 1		
fully reduced	$k_1 = 5.6 \times 10^7\ M^{-1}\ s^{-1}$	$k_{-1} = 6.2 \times 10^5\ s^{-1}$	$K_1 = k_1/k_{-1} = 90\ M^{-1}$
	$k_2 = 1.1 \times 10^3\ s^{-1}$	$k_{-2} = 0.023\ s^{-1}$	$K_2 = 4.8 \times 10^4$
	Scheme 2		
mixed-valence	$k_{1f} = 6.4 \times 10^7\ M^{-1}\ s^{-1}$	$k_{-1r} = 6.4 \times 10^5\ s^{-1}$	$K_1' = k_{1f}/k_{1r} = 100\ M^{-1}$
	$k_{2f} = 1.9 \times 10^5\ s^{-1}$	$k_{-2r} = 1.1 \times 10^4\ s^{-1}$	$K_2' = k_{2f}/k_{2r} = 17$
	$k_{3f} = 1.3 \times 10^4\ s^{-1}$	$k_{-3r} = 8.8 \times 10^3\ s^{-1}$	$K_3' = k_{3f}/k_{3r} = 1.5$
	$k_{4f} = 9.3 \times 10^2\ s^{-1}$	$k_{-4r} = 0.023\ s^{-1}$	$K_4' = k_{4f}/k_{4r} = 4.0 \times 10^4$
	$k_{5f} = 56\ s^{-1}$	$k_{-5r} = 82\ s^{-1}$	$K_5' = k_{5f}/k_{5r} = 0.68$

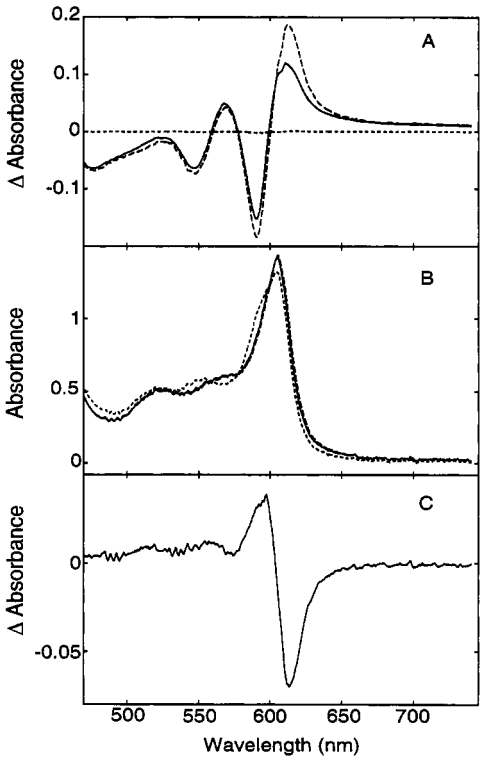

FIGURE 7: (A) Intermediate difference spectra of the fully reduced CO complex calculated from the b-spectra in Figure 2A, the mechanism in Scheme 1, and the associated microscopic rate constants (Table 1) (see text). The spectra represent the difference between the spectra of the intermediates in Scheme 1 and the spectrum of the fully reduced CO-bound complex. The dashed curve represents the intermediate **I** difference spectrum and the solid line the intermediate **II** difference spectrum. The dotted line along zero absorbance represents the intermediate difference spectrum of intermediate **O**. (B) The spectra of the intermediates present following photolysis of CO from the fully reduced enzyme (Scheme 1): intermediate **I** (dashed line), intermediate **II** (solid line), and intermediate **O** (dotted line). The spectra were obtained by adding the spectrum of the fully reduced CO-bound complex to the difference spectra in (A). (C) The spectrum of intermediate **II** minus that of intermediate **I**.

Scheme 1

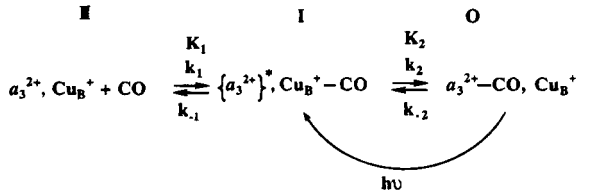

dashed line) has a significantly higher absorbance in the α band than that of intermediate **II** (Figure 7A, solid line), which has a spectrum nearly identical to the difference spectrum of the unliganded fully reduced enzyme and the fully reduced CO complex. This was used as a criterion for 100% photolysis and supports our earlier suggestion that the spectral change on a microsecond time scale is due to relaxation of cytochrome a_3 to its unliganded equilibrium state (Woodruff et al., 1991; Einarsdóttir et al., 1993). The dotted line along the zero absorbance in Figure 7A represents the intermediate **O** difference spectrum, i.e., the difference between the final product, the recombined CO complex, and the original fully reduced CO enzyme.

The absorption spectra of the intermediates present following photodissociation of CO from the fully reduced CO complex are shown in Figure 7B. They were obtained by adding the spectrum of the fully reduced CO complex to the intermediate difference spectra in Figure 7A. The absorbance spectra of intermediates **I** (dashed line) and **II** (solid line) are the same except the α band of the former is red shifted 1−2 nm relative to the latter. A 1−2 nm red shift of intermediate I relative to intermediate II was also noted in the Soret region (Georgiadis et al., 1994). The dotted line represents the spectrum of intermediate **O**, the fully reduced CO complex. Figure 7C represents the spectral change between intermediates **I** and **II**.

The nature of the conformational change in cytochrome a_3 in intermediate **I** is not known, but ligand exchange between cytochrome a_3^{2+} and Cu_B^+ (Woodruff et al., 1991; Einarsdóttir et al., 1993) or changes in the heme pocket causing tilt or rotation of the proximal histidine (Findsen et al., 1987; Lou et al., 1993) have been proposed.

Photolysis of the Mixed-Valence CO Complex. Previous studies of the CO photodissociation dynamics of the mixed-valence CO derivative have indicated that electron transfer from cytochrome a_3 to cytochrome *a* occurs on an early microsecond time scale ($\tau \sim 3-5\ \mu s$). This conclusion is based on absorbance changes observed at 605 and 445 nm (Oliveberg & Malmström, 1991) or at selected wavelengths in the Soret region (Verkhovsky et al., 1992) and, most recently, on global analysis of multichannel transient difference spectra in the Soret region (Georgiadis et al., 1994). As evident from the transient difference spectra in Figure 1C, there is a small absorbance increase in the α band on a microsecond time scale, indicative of the reduction of cytochrome *a*. However, this increase is accompanied by a significant blue shift in the α band, suggesting that an additional process occurs on a similar time scale. This is supported by the global analysis which indicates two processes on an early microsecond time scale with apparent lifetimes of 1.4 and 4.8 μs.

Kinetic Modeling. The global exponential fitting analysis of the transient difference spectra of the mixed-valence CO complex implies that at least five intermediates, in addition

Scheme 2

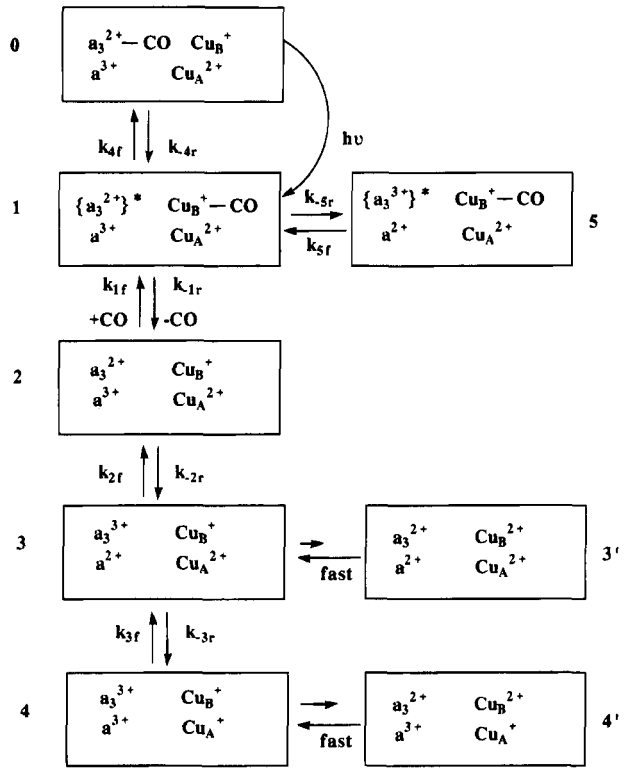

to the final product, are present. The analysis gives us the minimum number of processes involved, their associated b-spectra, and apparent rate constants (lifetimes). The second part of the analysis involves testing different mechanistic pathways and extracting the kinetics (the microscopic rate constants) and absorption spectra of the intermediates involved. Our kinetic model must account for the following observations: (1) an increase in the absorbance at 520 nm and a shift in the α band on an early microsecond time scale; (2) two early microsecond processes; (3) a decrease in the absorbance at 830 nm on a time scale of 50−100 μs, most likely due to the reduction of Cu_A; (4) the CO recombination on a millisecond time scale; and (5) a second millisecond process.

We have fitted our time-resolved data to the pathway in Scheme 2, which is consistent with the scheme used to fit the transient difference spectra in the Soret region (Georgiadis et al., 1994). The microscopic rate constants for the mixed-valence CO complex (Table 1) are similar to those observed in the Soret region (Georgiadis et al., 1994). The first step in Scheme 2 is attributed to a conformational change at cytochrome a_3 (Georgiadis et al., 1994). The second (**2** ↔ **3**) and third steps (**3** ↔ **4**) are attributed to electron transfer between the hemes and between cytochrome *a* and Cu_A, respectively, in agreement with the results of Oliveberg and Malmström (1991), Verkhovsky et al. (1992), and recent studies from our laboratory in the Soret region (Georgiadis et al., 1994). The second step (**2** ↔ **3**), the electron transfer from cytochrome a_3 to cytochrome *a*, is highly favorable in the physiological direction, i.e., in the direction of reduced cytochrome a_3 and oxidized cytochrome *a*, with a value of $K_2' = k_{2f}/k_{2r} = 17$. A value of 10 was used for the same process in the Soret region (Georgiadis et al., 1994). The equilibrium constant for the electron transfer between cytochrome *a* and Cu_A is 1.5 in favor of reduced cytochrome *a* and oxidized Cu_A. This value is identical to the value determined from the redox potentials of cytochrome *a* and Cu_A in the CO-inhibited enzyme (Ellis et al., 1986; Wang et al., 1986; Morgan et al., 1989). A corresponding value in the Soret region was 1.8 (Georgiadis et al., 1994).

The millisecond CO recombination originates from intermediate **1** (Georgiadis et al., 1994). The second millisecond process can be attributed either to electron transfer from cytochrome a_3 to cytochrome *a*, originating from intermediate **1**, or to electron transfer from Cu_B to oxidized cytochrome *a*, originating from intermediate **4**. The former possibility is represented in Scheme 2. The intermediates marked with a prime (′) in Scheme 2 represent species in which cytochrome a_3 is reduced and Cu_B is oxidized. Although electron transfer between cytochrome a_3 and Cu_B is expected to be too fast for our time resolution (τ <40 ns), the contribution of intermediates **3′** and **4′** to the transient data, and hence its incorporation into the calculated spectra, would depend on the relative midpoint potentials of the two metal centers in the respective redox states. In our modeling of the transient data, the two equilibria (**3** ↔ **3′** and **4** ↔ **4′**) were considered to be highly favored in the direction of oxidized cytochrome a_3 and reduced Cu_B. Consequently, any contribution of the spectra of intermediates **3′** and **4′** was omitted when the corresponding model spectra were calculated.

A higher redox potential of Cu_B over that of cytochrome a_3 in intermediate **3** (where cytochrome *a* is reduced) is supported by EPR redox titration studies which show a $g = 6$ signal, attributed to cytochrome a_3, upon partial reduction of the enzyme (Van Gelder & Beinert, 1969; Beinert et al., 1976; Beinert & Shaw, 1977; Shaw et al., 1978). In these studies, no EPR signal due to Cu_B^{2+} was detected, indicating that Cu_B is reduced and the magnetic coupling in the binuclear center is broken. The assumption that the potential of Cu_B (~340 mV) is significantly larger than that of cytochrome a_3 in intermediate **3** is also consistent with interpretations of potentiometric results in terms of negative redox cooperativity between the two hemes (the neoclassical model) (Nicholls & Petersen, 1974). In this model, the reduction of either heme would lead to a decrease in the redox potential of the other (Wikström et al., 1976; Carithers & Palmer, 1981). In a partially reduced state of the enzyme, like intermediate **3**, it follows that the oxidized cytochrome a_3 center would exhibit a significantly lower potential than in the resting enzyme, and therefore, the potential difference between cytochrome a_3 and Cu_B would be greater (assuming that the potential of Cu_B stays the same). The relative midpoint potentials of cytochrome a_3 and Cu_B in intermediate **4** are more obscure since the population of this state would be expected to be very small at equilibrium (Wikström et al., 1981). However, redox titrations with dithionite have indicated a significant increase in the intensity of the cytochrome a_3^{3+} $g = 6$ EPR signal in a time interval where the intensity of the $g = 3$ signal, attributed to the oxidized cytochrome *a*, decreased only slightly (Van Gelder & Beinert, 1969). This would suggest that a population of molecules in which cytochrome a_3 and cytochrome *a* are both oxidized and Cu_B is reduced, i.e., the state of intermediate **4**, can be present under nonequilibrium conditions. That Cu_B has a higher midpoint redox potential than cytochrome a_3 in both intermediates **3** and **4** is supported by our previous modeling in the Soret region (Georgiadis et al., 1994).

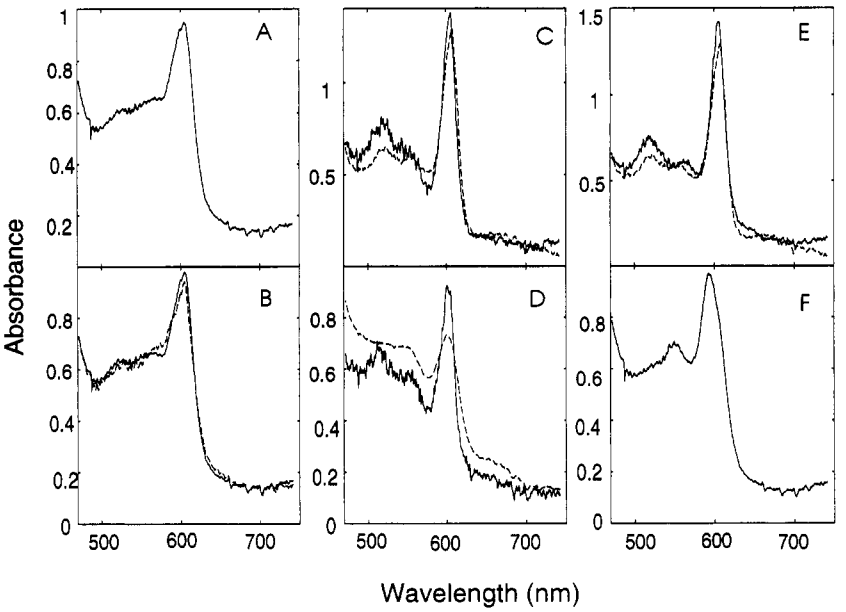

FIGURE 8: Comparison of the experimental (solid lines) and calculated (dashed lines) spectra of the intermediates present following photolysis of CO from the mixed-valence CO complex (Scheme 2). The experimental spectra were determined based on the mechanism in Scheme 2, the b-spectra in Figure 4, and the microscopic rate constants in Table 1. The calculated spectra were obtained by the appropriate linear combination of the ground state absorption spectra of oxidized, reduced, mixed-valence CO and fully reduced CO derivatives (see text for details). (A) The experimental spectrum of intermediate **1** in Scheme 2. (B) The experimental (solid line) and calculated (dashed line) spectra of intermediate **2** in Scheme 2. (C) The experimental (solid line) and calculated (dashed line) spectra of intermediate **3** in Scheme 2. (D) The experimental (solid line) and calculated (dashed line) spectra of intermediate **4** in Scheme 2. (E) The experimental (solid line) and calculated (dashed line) spectra of intermediate **5** in Scheme 2. (F) The experimental and calculated spectra of intermediate **0** in Scheme 2.

Intermediate Absorption Spectra. The difference spectra of the intermediates in Scheme 2 (the difference between the absorption spectra of the intermediates and the mixed-valence CO complex) were derived using Scheme 2, the b-spectra, and the microscopic rate constants in Table 1. The experimental absorption spectra of the intermediates were obtained by adding the spectrum of the mixed-valence CO complex to the intermediate difference spectra. The absolute spectra are shown in Figure 8 (solid lines). To evaluate the validity of the mechanism in Scheme 2, we have compared these spectra to calculated (model) spectra (Figure 8, dashed lines) which were obtained from appropriate linear combinations of ground state spectra of oxidized, reduced, mixed-valence CO and fully reduced CO enzyme derivatives (Georgiadis et al., 1994). The experimental spectrum of intermediate **1** in Scheme 2 is shown in Figure 8A. This spectrum was not modeled since we do not know the spectral profile of $\{a_3^{2+}\}^*$. The calculated spectrum of intermediate **2** (Figure 8B, dashed line), a_3^{2+} Cu_B^+ a^{3+} Cu_A^{2+}, was obtained by subtracting the spectrum of the fully reduced CO complex from the sum of the spectra of the mixed-valence CO derivative and the fully reduced unliganded enzyme. It should equal the experimental spectrum of intermediate **2** in Scheme 2 if spectral interactions between individual redox centers are ignored. The absorption spectrum of intermediate **3** (Figure 8C, solid line) in Scheme 2, a_3^{3+} Cu_B^+ a^{2+} Cu_A^{2+}, was modeled by subtracting the spectrum of the mixed-valence CO complex from that of the fully reduced CO complex and adding to the result the spectrum of the oxidized enzyme (Figure 8C, dashed line). This linear combination gives a_3^{3+} Cu_B^{2+} a^{2+} Cu_A^+. In this case, the redox states of the hemes are the same in the experimental and calculated spectra, whereas the redox states of the coppers are not. The experimental absorption spectrum of intermediate **4** in Scheme 2, a_3^{3+} Cu_B^+ a^{3+} Cu_A^+, is shown in Figure 8D (solid line). It was modeled by the spectrum of the fully oxidized resting enzyme, a_3^{3+} Cu_B^{2+} a^{3+} Cu_A^{2+} (Figure 8D, dashed line). Again, the redox states of the hemes are the same as those of intermediate **4** in Scheme 2, but the coppers are oxidized rather than reduced. The possibility that the oxidized cytochrome a_3 in intermediate **5** has a different structure than in intermediate **3** is represented by $\{a_3^{3+}\}^*$. Since we do not know the spectrum of $\{a_3^{3+}\}^*$, the spectrum of intermediate **5** was modeled by the calculated spectrum of intermediate **3** obtained as described above (Figure 8E). Figure 8F shows the spectrum of the final product, the mixed-valence CO complex. The experimental and model spectra of the mixed-valence CO complex were identical. Since the majority of the absorption in both the Soret and visible regions is expected to be due to the $\pi \rightarrow \pi^*$ transitions of the hemes, the calculated spectra would be expected to represent a reasonable model of the experimental spectra if (1) the mechanism in Scheme 2 is valid, (2) the microscopic rate constants in Table 1 are reasonable, and (3) if spectral interactions between individual redox centers and possible absorbance contribution from the coppers are ignored. As discussed below, the last assumption may not be valid.

The experimental absorption spectra of the intermediates represented in Scheme 2 differ somewhat from the calculated spectra (Figure 8). The spectrum of intermediate **2** has a slightly higher intensity in the α band than the corresponding model spectrum (Figure 8B). The α band in the experimental spectrum of intermediate **3** (Figure 8C, solid line) is blue shifted 1−2 nm relative to the corresponding model spectrum and has a slightly higher intensity. The experimental spectrum also has a significantly larger intensity between 480 and 550 nm than the calculated spectrum. In the case

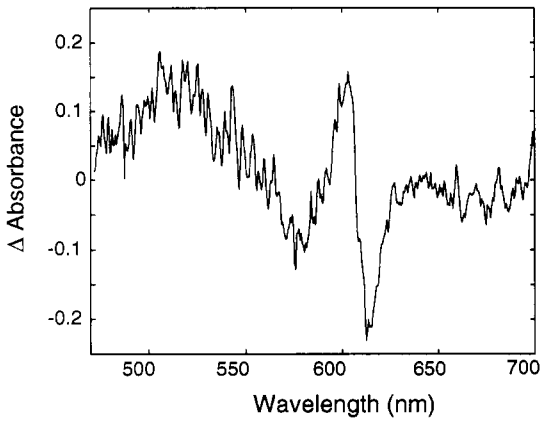

FIGURE 9: The difference between the experimental spectrum of intermediate **3**, a_3^{3+} Cu_B^{+} a^{2+} Cu_A^{2+} (Figure 8C, solid line), and the calculated spectrum, a_3^{3+} Cu_B^{2+} a^{2+} Cu_A^{+} (Figure 8C, dashed line). The result is equal to $Cu_A^{2+} - Cu_A^{+}$, $Cu_B^{+} - Cu_B^{2+}$.

of intermediate **4**, the experimental absorbance spectrum has a higher intensity at ~600 nm and a deeper trough at ~580 nm than the calculated spectrum (Figure 8D). There are also significant differences between 480 and 550 nm and substantially higher intensity at ~655 nm in the model spectrum.

The discrepancy between the experimental and model spectra of intermediate **3** (Figure 8C) in the 480−550 nm region might seem to contradict 1:1 electron transfer between the two hemes previously reported (Oliveberg & Malmström, 1991; Verkhovsky et al., 1992; Georgiadis et al., 1994) by suggesting that part of the absorbance increase at 520 nm might be due to another chromophore. Indeed, we previously suggested that a part of the absorbance increase at 520 nm might be due to Cu_B^{2+} being produced upon electron transfer to cytochrome *a* (Einarsdóttir et al., 1992a). However, we now believe there is an alternative explanation. As mentioned above, the experimental and calculated spectra of intermediate **3** differ in the redox states of the coppers. The difference between the experimental spectrum of intermediate **3** (Figure 8C, solid line), a_3^{3+} Cu_B^{+} a^{2+} Cu_A^{2+}, and the model spectrum, a_3^{3+} Cu_B^{2+} a^{2+} Cu_A^{+} (Figure 8C, dashed line), is equal to $Cu_A^{2+} - Cu_A^{+}$, $Cu_B^{+} - Cu_B^{2+}$. This difference spectrum is shown in Figure 9. Although Cu_B^{2+} has not been reported to have an absorption in the visible region [except possibly at 585 nm (Karlsson & Andréasson, 1981)], Cu_A^{2+} has been shown by low-temperature magnetic circular dichroism spectroscopy to have an absorption band with maximum at ~520 nm (Greenwood et al., 1983; Thomson et al., 1986; Greenwood et al., 1988; Farrar et al., 1991). Therefore, we assign the absorbance between 480 and 550 nm in Figure 9 to Cu_A^{2+}. The extinction coefficient at 520 nm, ϵ ~3000 M^{-1} cm^{-1}, is reasonable for a copper-to-ligand charge transfer transition (Solomon et al., 1980). Our assignment is supported by the visible spectrum of a Cu_A mutant of subunit II of cytochrome *bo* from *E. coli* (van der Oost et al., 1992; Kelly et al., 1993), which shows an absorbance band between 480 and 550 nm. The visible spectra of the Cu_A domains of cytochrome *c* oxidase from *P. denitrificans* (Lappalainen et al., 1993) and *caa*$_3$ oxidase from *B. subtilis* (von Wachenfeldt et al., 1994) also show absorbances in this region. These spectra are similar to the spectrum of nitrous oxide reductase and, together with other spectroscopic evidence, provide further support for Cu_A being a mixed-valence copper center (Scott et al., 1989; Kroneck et al., 1990; Antholine et al., 1992). The peak at ~605 nm and the trough at ~615 nm in the difference spectrum in Figure 9 are not attributed to Cu_A^{2+} or Cu_B^{2+}, but are believed to result from spectral interactions between the individual redox centers (see below) (Blair et al., 1982; Georgiadis et al., 1994). The difference between the calculated absorption spectrum of intermediate **4**, a_3^{3+} Cu_B^{2+} a^{3+} Cu_A^{2+}, and the experimental absorption spectrum, a_3^{3+} Cu_B^{+} a^{3+} Cu_A^{+}, in the 480−550 nm region is similarly attributed to Cu_A^{2+}.

Electron transfer from cytochrome *a* to Cu_A in Scheme 2 (**3** ↔ **4**) is supported by the near-infrared transient difference spectrum which shows a decrease at 830 nm on the 50−100 μs time scale (Figure 6B). Using the extinction coefficient of 2.3 mM^{-1} cm^{-1} at 830 nm for the reduced-minus-oxidized spectrum (Boelens et al., 1982), the amount of Cu_A being reduced, based on the spectral changes in Figure 6B, was estimated to be ~2−3%. This value is in good agreement with the small population of intermediate **4** (3.2%) calculated based on Scheme 2 and the microscopic rate constants listed in Table 1.

Included in Scheme 2 is the equilibrium between cytochrome a_3 and Cu_B (**3** ↔ **3′** and **4** ↔ **4′**). As discussed above, the two equilibria are expected to lie in favor of reduced Cu_B and oxidized cytochrome a_3. This is supported by the fact that the correspondence between the experimental and calculated spectra of intermediates **3** and **4** was not significantly improved by model spectra which are a mixture of intermediates **3** and **3′** and intermediates **4** and **4′**, respectively. This was also found to be the case for the Soret region (Georgiadis et al., 1994). However, our data do not exclude a small fraction of molecules in which cytochrome a_3 is reduced and Cu_B oxidized (<20%).

Three-Electron-Reduced CO Complex. The transient data of the three-electron-reduced CO complex support the mechanism in Scheme 2 for the mixed-valence CO enzyme. The microsecond time scale transient difference spectra of the three-electron-reduced CO enzyme (Figure 5A) appear to be a mixture of the corresponding spectra of the fully reduced (Figure 1A) and the mixed-valence CO enzyme derivatives (Figure 1C). A decrease is observed in the α band on an early microsecond time scale (Figure 5A) analogous to that observed in the fully reduced CO enzyme (Figure 1A). However, the decrease is smaller than in the fully reduced enzyme due to simultaneous heme-to-heme electron transfer spectral changes. The b-spectrum associated with the ~5 μs lifetime is smaller in the three-electron-reduced CO enzyme than the corresponding b-spectrum for the mixed-valence CO complex. Conversely, electron transfer from cytochrome *a* to Cu_A occurs to a greater extent following photodissociation of CO from the three-electron reduced CO complex compared to the mixed-valence CO compound. This is reflected by a larger decrease at 830 nm in the three-electron-reduced CO complex, in agreement with previous studies (Morgan et al., 1989; Oliveberg & Malmström, 1991). This is also supported by a significantly larger b-spectrum associated with the 77 μs phase in the three electron-reduced CO derivative (Figure 5C, unbold dotted line) compared to the mixed-valence complex (Figure 4A, unbold dotted line). This is to be expected since species with partially reduced cytochrome *a* and Cu_A dominate in the three-electron-reduced CO derivative (Morgan et al., 1989; Oliveberg & Malmström, 1991). Due to intramolecular redox equilibria, the population of molecules at the three-

electron level of reduction should theoretically account for 50% of the molecules in the three-electron-reduced CO complex (Morgan et al., 1989). However, due to redox anticooperativity between cytochrome *a* and Cu_A, this number has been suggested to be closer to 69% (Copeland et al., 1987). Other populations in the three-electron-reduced enzyme would be the fully reduced CO derivative and the mixed-valence CO complex. Therefore, a mechanistic scheme for the three-electron-reduced CO derivative would be expected to be significantly more complicated than for the mixed-valence CO complex. It could possibly involve three sequential pathways, a pathway for the fully reduced CO complex (Scheme 1), a pathway for the mixed-valence CO population (Scheme 2), and a pathway for the population of molecules at the three-electron level of reduction, which would presumably involve a conformational change at cytochrome a_3 followed by electron transfer from cytochrome *a* to Cu_A.

The results from our global analysis show two millisecond processes in addition to the three microsecond processes, in agreement with our results on the mixed-valence CO complex in the Soret region (Georgiadis et al., 1994) and recent results of Hallén et al. (1994). One of these processes is attributed to the CO recombination, which originates from intermediate **1** (Scheme 2) since CO must bind to Cu_B^+ prior to recombining with cytochrome a_3 (Woodruff et al., 1991; Einarsdóttir et al., 1993). Our kinetic modeling shows that the rate constants for the CO recombination in the fully reduced CO enzyme and the mixed-valence CO derivative are the same (compare k_2 and k_{4f} in Table 1). The origin of the second millisecond process is unknown, but it could reflect intramolecular electron transfer between the two hemes as suggested recently by Hallén et al. (1994). In Scheme 2, we have postulated that the millisecond process represents electron transfer from cytochrome a_3 to cytochrome *a* originating from intermediate **1** rather than intermediate **2** (Scheme 2, **1** ↔ **5**). There is good agreement between the experimental and model spectra of intermediate **5** (Figure 8E). Therefore, different conformations of cytochrome a_3 in intermediate **1** and intermediate **2** may account for the 10^3-10^4-fold difference in electron transfer rates between cytochrome a_3 and cytochrome *a* in intermediates **1** and **2** (Table 1). Alternatively, the second millisecond process could reflect electron transfer from Cu_B to cytochrome *a* originating from intermediate **4**. Our data alone do not allow us to distinguish between the two alternatives, since in both cases the resultant intermediate would have cytochrome a_3 oxidized and cytochrome *a* reduced. However, in view of recent site-directed mutagenesis studies of cytochrome *bo* from *E. coli* and cytochrome aa_3 from *Rhodobacter sphaeroides* (Hosler et al., 1993), which have indicated that cytochrome a_3 is situated between Cu_B and cytochrome *a*, electron transfer between the two hemes seems like the more attractive possibility.

The different conformations of cytochrome a_3 in intermediates **1** and **5** compared to those in intermediates **2** and **3**, respectively, also appear to result in different relative redox midpoint potentials (and hence different equilibrium constants) of cytochrome a_3 and cytochrome *a* for the two heme-to-heme electron transfer processes. For the millisecond process (Scheme 2, **1** ↔ **5**) the calculated equilibrium constant is 1.5 in the direction of oxidized cytochrome a_3 and reduced cytochrome *a*, whereas in the case of the microsecond process the reaction is highly favored in the direction of reduced cytochrome a_3 and oxidized cytochrome *a* (Table 1).

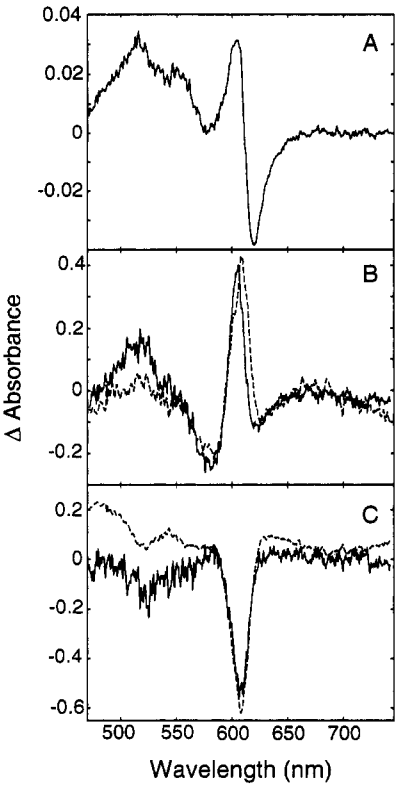

FIGURE 10: (A) The difference between the experimental spectra of intermediates **1** and **2** (Scheme 2) in Figure 9. (B and C) Comparison of the experimentally determined spectral differences for the two electron transfer steps in Scheme 2 (solid lines) with the calculated difference spectra (dotted lines). The calculated spectra were determined from the ground state absorption spectra of the oxidized, reduced, fully reduced CO and the mixed-valence CO enzyme derivatives. (B) Spectral changes associated with the electron transfer between the two hemes and (C) between cytochrome *a* and Cu_A (see text for details).

Spectral Interactions. The experimental spectral change associated with the conformational change in the mixed-valence CO enzyme (Scheme 2, **2** minus **1**) is shown in Figure 10A. It is clear that this spectral change is similar, but not identical, to that observed for the fully reduced CO compound (Figure 7C). The difference is attributed to the effect of the redox state of cytochrome *a* and/or Cu_A on the spectrum of cytochrome a_3 in intermediates **1** and **2**. This is supported by recent resonance Raman studies of the CO photodissociation dynamics of the mixed-valence CO and the fully reduced CO complexes, which have indicated that the redox states of cytochrome *a* and/or Cu_A modulate the distal heme pocket dynamics (Lou et al., 1993). Figure 10B shows a comparison between the experimental (solid line) and calculated (dotted line) spectral change associated with the electron transfer between cytochrome a_3 and cytochrome *a*. The difference between the experimental and calculated spectra of intermediates **2** and **3** (Figure 8B and 8C) manifests itself as a shift in the α band between the experimental and calculated difference spectra (Figure 10B). The difference between the experimental spectral change, $(a^{2+} - a^{3+})$ minus $(a_3^{2+} - a_3^{3+})$, and the calculated spectral change, $(a^{2+}\ Cu_A^{+} - a^{3+}\ Cu_A^{2+})$ minus $(a_3^{2+}\ Cu_B^{+} - a_3^{3+}\ Cu_B^{2+})$, in the 480−550 nm region, attributed to Cu_A^{2+}, is also clearly observed (Figure 10B).

The discrepancy between the experimental and calculated spectra of intermediates **3** and **4** (Figure 8C,D) is also attributed to spectral interactions among the redox centers. In the calculated spectra, the redox centers are assumed to be spectrally independent, i.e., the absorbance spectrum of each of the metal centers is considered to be independent of the ligation or oxidation state of the other redox centers. A closer look at the differences between the experimental and calculated spectra of intermediates **3** and **4** can give some insight into which redox centers are involved. When the spectral change associated with the oxidation of cytochrome *a* and reduction of Cu_A (Scheme 2, **4** minus **3**) is compared to the calculated spectral change (Figure 10C), the difference in the α band between the experimental and calculated spectra of intermediates **3** and **4** (Figure 8C and 8D) disappears, and only the difference between the two between 480 and 550 nm is observed (Figure 10C). This indicates that the difference in the α band between the experimental and calculated spectra of intermediate **3** is the same as the spectral difference between the experimental and calculated absorption spectra of intermediate **4**. This is supported by the following observation. If the experimental spectrum of intermediate **4** is used to calculate the spectrum of intermediate **3**, i.e., the spectrum of intermediate **4** rather than that of the fully oxidized resting enzyme is added to the difference spectrum of the fully reduced CO minus the mixed-valence CO enzyme, the experimental and the calculated spectra of intermediate **3** match in the α band (they still differ in the 480−550 nm region as expected) when the mechanism in Scheme 2 and the microscopic rate constants in Table 1 are used (not shown). The difference between the experimental and calculated spectra of intermediate **3** and the corresponding difference for intermediate **4** were also found to be very similar for the data in the Soret region [see Georgiadis et al. (1994), Figure 9].

These results indicate that the spectral interactions are the same in intermediates **3** and **4** and therefore due to metal centers whose redox states are unchanged between the two intermediates. Since both cytochrome *a* and Cu_A undergo a redox change between intermediates **3** and **4**, the difference between the experimental and calculated spectra of intermediates **3** and **4** (Figure 8C,D) is most likely due to the effect of the redox state of Cu_B on the absorbance spectrum of cytochrome a_3 which is oxidized in both intermediates. Cu_B is in its reduced state in intermediates **3** and **4** in Scheme 2, whereas it is oxidized in the corresponding model spectra. Therefore, if the redox state of Cu_B has an effect on the spectrum of the oxidized cytochrome a_3, a discrepancy would be expected between the experimental and calculated spectra of intermediates **3** and **4**. Previous studies have indicated that the extinction coefficient of cytochrome a_3 in the visible region may be significantly affected by the redox state of Cu_B, possibly through electrostatic interactions (Blair et al., 1982). On the basis of previous EPR redox titration results on the partially reduced enzyme, the magnetic coupling between cytochrome a_3 and Cu_B would be broken by the reduction of Cu_B in intermediates **3** and **4**, and a $g = 6$ signal would be expected (Van Gelder & Beinert, 1969; Beinert et al., 1976; Beinert & Shaw, 1977; Shaw et al., 1978). The loss of magnetic coupling in the binuclear center could undoubtedly affect the spectrum of cytochrome a_3. The spectral band at 655 nm has been found to have a reciprocal relationship with the rhombic signal at $g = 6$ (Beinert et al., 1976), and it has been attributed to cytochrome a_3 magnetically coupled to Cu_B (Beinert et al., 1976; Mitchell et al., 1991). The lack of the 655 nm band in the experimental spectrum of intermediate **4** reflects that Cu_B is reduced and/or that the antiferromagnetic coupling between cytochrome a_3 and Cu_B is broken. A support for a larger extinction coefficient of the α band of cytochrome a_3 in intermediate **4** compared to that of the resting state comes from the EPR redox titration with dithionite referred to above (Van Gelder & Beinert, 1969). In this experiment a significant intensity of the $g = 6$ signal was observed concomitant with a large increase in the α band. However, the value of the $g = 3$ signal decreased only slightly. This suggests that the increase in the α band is not only due to the reduction of cytochrome *a* but also due to oxidation of cytochrome a_3 when Cu_B is reduced.

The difference between the experimental and calculated absorption spectra of intermediates **3** and **4** may reflect the fact that cytochrome a_3 is not in its oxidized resting equilibrium state but rather in a transient "pulsed-like" conformation (Antonini et al., 1977; Rosén et al., 1977; Brunori et al., 1979), which may or may not be due the redox state of Cu_B as discussed above. This is supported by a higher α band intensity and a deeper trough at ~580 nm in the experimental spectrum of intermediate **4** (Figure 8D), and the absence of a significant absorption at 655 nm in the spectra of intermediates **3** and **4** (Rosén et al., 1977; Brunori et al., 1979; Armstrong et al., 1983). The pulsed cytochrome oxidase is formed following reduction by dithionite and subsequent oxidation by dioxygen (Antonini et al., 1977; Brunori et al., 1979), but can also be obtained by oxidizing the reduced enzyme by ferricyanide or porphyrexide (Beinert et al., 1976; Beinert & Shaw, 1977; Shaw et al., 1978; Brunori et al., 1981; Armstrong et al., 1983). The form produced by the anaerobic oxidation is also characterized by the generation of the $g = 6$ signal (Beinert et al., 1976; Shaw et al., 1978), suggesting that Cu_B is reduced in the pulsed enzyme. Since cytochrome a_3 started out oxidized before the mixed-valence CO complex was produced, it has already undergone one turnover cycle in intermediates **3** and **4** and could potentially be in a pulsed-like conformation. The experimental spectrum of intermediate **4** and the spectrum of the pulsed enzyme, generated upon reoxidation of the reduced enzyme by dioxygen (data not shown), are in better agreement than when the spectrum of the resting enzyme is used.

CONCLUSIONS

We conclude from our global analysis of the transient data in the visible region that at least two intermediates (in addition to the final products) are present in the photodissociation dynamics of the fully reduced CO complex. Five intermediates are present in the case of the mixed-valence CO compound. These results are supported by global analysis of the transient data in the Soret region (Georgiadis et al., 1994). On the basis of the mechanisms in Schemes 1 and 2 we have determined the visible absorption spectra of the intermediates involved in the CO photodissociation dynamics of the fully reduced CO complex and the mixed-valence CO enzyme, respectively. The good correspondence between the experimental and calculated spectra of the mixed-valence CO complex in both the visible and Soret regions (Georgiadis et al., 1994) argues strongly in favor of

the mechanism in Scheme 2. The difference between the experimental and model spectra in the 480−550 nm region has allowed us to extract the absorbance spectrum of Cu_A^{2+}. Our results also indicate that the redox state of Cu_B may have a significant effect on the extinction coefficient of oxidized cytochrome a_3 in the visible region. Spectral interactions between cytochrome a_3 and Cu_B are also supported by our previously published data in the Soret region (Georgiadis et al., 1994).

The microscopic rate constants in Table 1 for the mixed-valence CO complex in the visible region are similar, although not identical, to those reported previously in the Soret region. The most noticeable difference is in the equilibrium constant of the heme-to-heme electron transfer step, $K_2' = k_{2f}/k_{2r}$, which is 10 for the Soret region (Georgiadis et al., 1994) and 17 for the visible region (Table 1). This difference could be due in part to photoreduction of cytochrome *a* which appears to occur to a greater extent in more dilute samples (those used for collecting data in the Soret region) than in more concentrated ones. Alternatively, the equilibrium constant for the visible region may in fact be lower than 17. A model in which the equilibrium constants for the two electron transfer steps in Scheme 2, K_2' and K_3', were 11.6 and 1.1 fitted the transient data nearly as well (data not shown) as when the equilibrium constants K_2' and K_3' were 17 and 1.5 (Table 1) based on the criteria used to select the optimal microscopic rate constants. For both sets of microscopic rate constants, there is a significantly higher intensity in the α band in the experimental spectrum of intermediate **4** than in the corresponding calculated spectrum, a considerably higher intensity in the 480−550 nm region in the experimental spectrum of intermediate **3** spectrum than in the calculated spectrum, and the near absence of the 655 nm band in the experimental spectrum of intermediate **4**. Therefore, both sets of equilibrium constants are consistent with the absorbance of Cu_A^{2+} between 480 and 550 nm, and both indicate significant spectral interactions between cytochrome a_3 and Cu_B.

Our results are in good agreement with previous studies of the CO photodissociation dynamics of the mixed-valence CO complex, which reported two apparent lifetimes of 3−5 and 35−80 μs, attributed to heme-to-heme electron transfer and electron transfer between cytochrome *a* and Cu_A, respectively (Oliveberg & Malmström, 1991; Verkhovsky et al., 1992). Electron transfer between the high and low spin hemes also occurs on a microsecond time scale upon photolysis of CO from wild-type cytochrome *bo* and cytochrome oo_3 from *E. coli* and mutant variants of cytochrome *bo* (Morgan et al., 1993; Brown et al., 1994). In addition to the two electron transfer processes, our data also show that a conformational change, presumably at cytochrome a_3, occurs prior to the first electron transfer step. Therefore, a conformational change may be a prerequisite for fast intramolecular electron transfer as suggested earlier by Brzezinski and Malmström (1987). Our analysis also provides evidence for a millisecond process, which we attribute to intramolecular electron transfer between cytochrome a_3 and cytochrome *a*, when the former is in a transient reduced conformation and not in its equilibrium unliganded conformation. A millisecond process, sensitive to pH and D_2O, was recently reported for the photolyzed mixed-valence CO complex (Hallén et al., 1994). The process was attributed to heme-to-heme electron transfer and was postulated to be coupled to protonation of a group close to the bimetallic site.

ACKNOWLEDGMENT

We thank Dr. Thorgeir Thorgeirsson for providing programs for the global exponential fitting analysis and for helpful discussions.

REFERENCES

Antholine, W. E., Kastrau, D. H. W., Steffens, G. C. M., Buse, G., Zumft, W. G., & Kroneck, P. M. H. (1992) *Eur. J. Biochem. 209*, 875−881.

Antonini, E., Brunori, M., Colosimo, A., Greenwood, C., & Wilson, M. T. (1977) *Proc. Natl. Acad. Sci. U.S.A. 74*, 3128−3132.

Armstrong, F., Shaw, R. W., & Beinert, H. (1983) *Biochim. Biophys. Acta 722*, 61−71.

Beinert, H., & Shaw, R. W. (1977) *Biochim. Biophys. Acta 462*, 121−130.

Beinert, H., Hansen, R. E., & Hartzell, C. R. (1976) *Biochim. Biophys. Acta 423*, 339−355.

Beinert, H., Shaw, R. W., Hansen, R. E., & Hartzell, C. R. (1980) *Biochim. Biophys. Acta 591*, 458−470.

Blair, D. F., Bocian, D. F., Babcock, G. T., & Chan, S. I. (1982) *Biochemistry 21*, 6928−6935.

Boelens, R., & Wever, R. (1979) *Biochim. Biophys. Acta 547*, 296−310.

Boelens, R., Wever, R., & Van Gelder, B. F. (1982) *Biochim. Biophys. Acta 682*, 264−272.

Brown, S., Rumbley, J. N., Moody, A. J., Thomas, J. W., Gennis, R. B., & Rich, P. R. (1994) *Biochim. Biophys. Acta 1183*, 521−532.

Brunori, M., Colosimo, A., Rainoni, G., Wilson, M. T., & Antonini, E. (1979) *J. Biol. Chem. 254*, 10769−10775.

Brunori, M., Colosimo, A., Sarti, P., Antonini, E., & Wilson, M. T. (1981) *FEBS Lett. 126*, 195−198.

Brzezinski, P., & Malmström, B. G. (1987) *Biochim. Biophys. Acta 894*, 29−38.

Carithers, R. P., & Palmer, G. (1981) *J. Biol. Chem. 256*, 7967−7976.

Copeland, R. A., Smith, P. A., & Chan, S. I. (1987) *Biochemistry 26*, 7311−7316.

Eglinton, D. G., Johnson, M. K., Thomson, A. J., Gooding, P. E., & Greenwood, C. (1980) *Biochem. J. 191*, 319−331.

Einarsdóttir, Ó., Dawes, T. D., & Georgiadis, K. E. (1992a) *Proc. Natl. Acad. Sci. U.S.A. 89*, 6934−6937.

Einarsdóttir, Ó., Georgiadis, K. E., & Dawes, T. D. (1992b) *Biochem. Biophys. Res. Commun. 184*, 1035−1041.

Einarsdóttir, Ó., Dyer, R. B., Lemon, D. D., Killough, P. M., Hubig, S. M., Atherton, S. J., López-Garriga, J. J., Palmer, G., & Woodruff, W. H. (1993) *Biochemistry 32*, 12013−12024.

Ellis, W. R., Jr., Wang, H., Blair, D. F., Gray, H. B., & Chan, S. I. (1986) *Biochemistry 25*, 161−167.

Farrar, J. A., Thomson, A. J., Cheesman, M. R., Dooley, D. M., & Zumft, W. G. (1991) *FEBS Lett. 294*, 11−15.

Findsen, E. W., Centeno, J., Babcock, G. T., & Ondrias, M. R. (1987) *J. Am. Chem. Soc. 109*, 5367−5372.

Georgiadis, K. E., Jhon, N.-I., & Einarsdóttir, Ó. (1994) *Biochemistry 33*, 9245−9256.

Golub, G. H., & Reinsch, C. (1970) *Numer. Math. 14*, 403−420.

Greenwood, C., Hill, B. C., Barber, D., Eglington, D. G., & Thomson, A. J. (1983) *Biochem. J. 215*, 303−316.

Greenwood, C., Thomson, A. J., Barrett, C. P., Peterson, J., George, G. N., Fee, J. A., & Reichardt, J. (1988) *Ann. N.Y. Acad. Sci. 550*, 47−52.

Hallén, S., Brzezinski, P., & Malmström, B. G. (1994) *Biochemistry 33*, 1467−1472.
Henry, E. R., & Hofrichter, J. (1992) *Methods Enzymol. 210*, 129−193.
Hosler, J. P., Ferguson-Miller, S., Calhoun, M. W., Thomas, J. W., Hill, J., Lemieux, L., Ma, J., Georgiou, C., Fetter, J., Shapleigh, J., Tecklenburg, M. M. J., Babcock, G. T., & Gennis, R. B. (1993) *J. Bioenerg. Biomembr. 25*, 121−136.
Hug, S. J., Lewis, J. W., Einterz, C. M., Thorgeirsson, T. E., & Kliger, D. S. (1990) *Biochemistry 29*, 1475−1485.
Ingledew, W. J., Bacon, M., & Rich, P. R. (1992) *FEBS Lett. 305*, 167−170.
Karlsson, B., & Andréasson, L.-E. (1981) *Biochim. Biophys. Acta 635*, 73−80.
Kelly, M., Lappalainen, P., Talbo, G., Haltia, T., van der Oost, J., & Saraste, M. (1993) *J. Biol. Chem. 268*, 16781−16787.
Kroneck, P. M. H., Antholine, W. E., Kastrau, D. H. W., Buse, G., Steffens, G. C. M., & Zumft, W. G. (1990) *FEBS Lett. 268*, 274−276.
Lappalainen, P., Aasa, R., Malmström, B. G., & Saraste, M. (1993) *J. Biol. Chem. 268*, 26416−26421.
Lou, B.-S., Larsen, R. W., Chan, S. I., & Ondrias, M. R. (1993) *J. Am. Chem. Soc. 115*, 403−407.
Mitchell, R., Mitchell, P., & Rich, P. R. (1991) *FEBS Lett. 280*, 321−324.
Morgan, J. E., Li, P. M., Jang, D.-J., El-Sayed, M. A., & Chan, S. I. (1989) *Biochemistry 28*, 6975−6983.
Morgan, J. E., Verkhovsky, M. I., Puustinen, A., & Wikström, M. (1993) *Biochemistry 32*, 11413−11418.
Nicholls, P., & Petersen, L. C. (1974) *Biochim. Biophys. Acta 357*, 462−467.
Oliveberg, M., & Malmström, B. G. (1991) *Biochemistry 30*, 7053−7057.
Rich, P. R., Moody, A. J., & Ingledew, W. J. (1992) *FEBS Lett. 305*, 171−173.
Rosén, S., Brändén, R., Vänngård, T., & Malmström, B. (1977) *FEBS Lett. 74*, 25−30.
Scott, R. A., Zumft, W. G., Coyle, C. L., & Dooley, D. M. (1989) *Proc. Natl. Acad. Sci. U.S.A. 86*, 4082−4086.
Shaw, R. W., Hansen, R. E., & Beinert, H. (1978) *Biochim. Biophys. Acta 504*, 187−199.
Solomon, E. I., Hare, J. W., Dooley, D. M., Dawson, J. H., Stephens, P. H., & Gray, H. B. (1980) *J. Am. Chem. Soc. 102*, 168−178.
Thomson, A. J., Greenwood, C., Peterson, J., & Barrett, C. P. (1986) *J. Inorg. Biochem. 28*, 195−205.
Thorgeirsson, T. E., Milder, S. J., Miercke, L. J. W., Betlach, M. C., Shand, R. F., Stroud, R. M., & Kliger, D. S. (1991) *Biochemistry 30*, 9133−9142.
Thorgeirsson, T. E., Lewis, J. W., Wallace-Williams, S. E., & Kliger, D. S. (1992) *Photochem. Photobiol. 56*, 1135−1144.
van der Oost, J., Lappalainen, P., Musacchio, A., Warne, A., Lemieux, L., Rumbley, J., Gennis, R. B., Aasa, R., Pasher, T., Malmström, B. G., & Saraste, M. (1992) *EMBO J. 11*, 3209−3217.
Van Gelder, B. F., & Beinert, H. (1969) *Biochim. Biophys. Acta 189*, 1−24.
Verkhovsky, M. I., Morgan, J. E., & Wikström, M. (1992) *Biochemistry 31*, 11860−11863.
von Wachenfeldt, C., De Vries, S., & van der Oost, J. (1994) *FEBS Lett. 340*, 109−113.
Wang, H., Blair, D. F., Ellis, W. R. J., Gray, H. B., & Chan, S. I. (1986) *Biochemistry 25*, 167−172.
Wharton, D. C., & Tzagoloff, A. (1964) *J. Biol. Chem. 239*, 2036−2041.
Wikström, M. K. F., Harmon, J. H., Ingledew, W. J., & Chance, B. (1976) *FEBS Lett. 65*, 259−277.
Wikström, M., Krab, K., & Saraste, M. (1981) *Cytochrome Oxidase—A Synthesis*, Academic Press, New York.
Woodruff, W. H., Einarsdóttir, Ó., Dyer, R. B., Bagley, K. A., Palmer, G., Atherton, S. J., Goldbeck, R. A., Dawes, T. D., & Kliger, D. S. (1991) *Proc. Natl. Acad. Sci. U.S.A. 88*, 2588−2592.
Yoshikawa, S., Choc, M. G., O'Toole, M. C., & Caughey, W. S. (1977) *J. Biol. Chem. 252*, 5498−5508.

BI941932G